# Spike-Feature Based Estimation of Electrode Position in Extracellular Neural Recordings

Thorbergsson, Palmi Thor; Garwicz, Martin; Schouenborg, Jens; Johansson, Anders J

# Spike-Feature Based Estimation of Electrode Position in Extracellular Neural Recordings

P. T. Thorbergsson, *Student Member, IEEE*, M. Garwicz,
J. Schouenborg, A. J Johansson, *Member, IEEE*

*Abstract*— Detecting and sorting spikes in extracellular neural recordings are common procedures in assessing the activity of individual neurons. In chronic recordings, passive electrode movements introduce changes in the shape of detected spike waveforms, and may thus lead to problems with identification and tracking of spikes recorded at separate instances in time, which is an important step in long-term monitoring of individual neurons. Information about electrode movements after implantation is crucial to the evaluation of mechanical stability of different electrode designs. In this paper, we present a preliminary study of the relationship between electrode movements and the resulting movements of spike-features in feature space. We show that there is a characteristic relationship between the two movements and that this relationship can be modeled as a linear transformation between two coordinate systems. Finally, we show how the relationship can be used for estimating electrode positions based on measured spike waveforms without any prior knowledge about the type of neuron by introducing a learning procedure during electrode insertion.

## I. INTRODUCTION

Extracellular recordings with chronically implanted microelectrodes are a common means of acquiring signals reflecting the activity of individual neurons in the central nervous system [1]. The recorded signal then consists of the spiking activity of near-by neurons (target neurons), the combined spiking activity of a large number of far-away neurons (noise neurons), thermal noise generated in the front-end electronics and local field potentials [2], [3].

When the target neurons are sufficiently close to the recording electrode, their spikes can be detected [4] and sorted [5] in order to reveal the firing patterns of individual neurons. Assuming that the detection has been successful, the sorting step involves extracting features from the spike waveforms and classifying similar waveforms as originating from the same neuron. Feature extraction is commonly carried out by projecting the spike waveforms onto a set of basis waveforms that can be obtained through e.g. principal component analysis (PCA) of the acquired spike waveforms.

Differences in spike waveforms arise from differences in neuron morphology and differences in electrode position relative to the different neurons [6], [7]. While spike sorting

relies on these differences, they can become problematic in dynamic situations, i.e. where the recording electrode can move in relation to the target neuron(s). This becomes especially challenging when comparing identified units in recordings from a specific electrode that are executed at separate time instances. While small electrode movements can slightly change the feature space representation of detected spikes from a given neuron, larger movements can put that neuron out of range from the electrode and new neurons into range. Solving this problem is commonly referred to as spike-tracking [8], [9] and involves comparing units between separate recording instances and concluding that they either originate in the same neuron or in different neurons.

Gaining insight into how electrode movements are translated into spike movements in feature space would be of great benefit both in terms of solving the spike-tracking problem and in terms of being able to estimate electrode movements based on observed spike waveforms. In this paper, we present a preliminary study of the relationship between physical movements of the recording electrode and the corresponding movements of spike-features in feature space. Using mathematical models to simulate multi-electrode recordings, we demonstrate how electrode movements along a given path are translated into spike-feature movements along a similar path in feature space. Exploring this insight, we present a method for using recorded spike waveforms to estimate the electrode position, based on the relationship between the two domains. Our results show that there is a characteristic relationship between electrode movements in the physical domain and spike-feature movements in the feature domain. This relationship is evident even when employing sub-optimal feature spaces. Our results also show that recorded spike waveforms provide information about the recording electrode position if a training procedure is carried out during implantation of the electrode.

## II. METHODS

### A. Dataset

As test data, we used synthetic multi-electrode recordings where the electrode sites were placed along the paths of electrode movements we wished to test in each case. We used a recently developed simulation tool that employs dimensionality reduction techniques to compactly describe the spatial dependency of the measured spike waveform. This allows for an efficient simulation of multielectrode recordings with realistic properties [10]. The model was derived by compressing the information obtained when calculating spike waveforms in measurement points
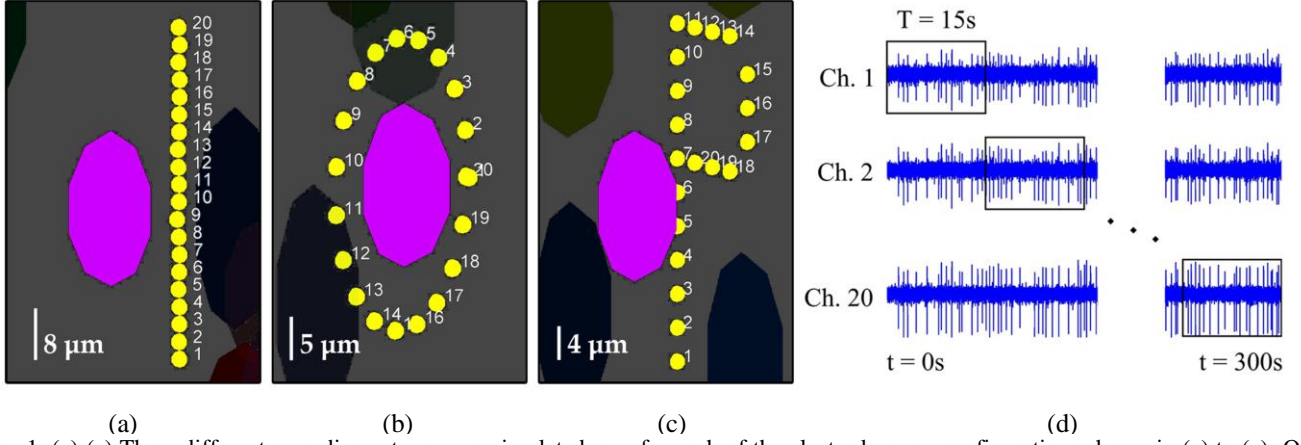
Fig. 1. (a)-(c) Three different recording setups were simulated, one for each of the electrode array configurations shown in (a) to (c). One target neuron (purple ellipsoid) was placed close to the electrode array and approximately 500 interfering neurons (dark ellipsoids) were placed at random positions at least 150μm away from the target neuron. (d) The effects of electrode movements were mimicked by extracting spikes from the recording channels from a time frame of length T s (T = 15s in the figure) while successively sweeping the window across the channels.

surrounding a compartment model of a CA1 pyramidal neuron using the simulation environment NEURON [6], [11], [12].

Fig. 1 shows the target neuron and the electrode locations considered for each of the three test recordings. The electrode paths we considered were 1) linear movement, 2) movement along an ellipse and 3) movement along a P-shaped path. Fig. 1 (d) shows how electrode movement was mimicked by extracting spikes in a time frame of duration T that was swept across the channels. This corresponds to the assumption that the electrode stays in place for the duration of the window, T. The linear movement was assumed to represent the practical case where electrodes are inserted and then assumed to move along one axis. The elliptic and P-shaped paths were included to show that complex electrode movements were translated to similar movements of spikes in the feature space.

Twenty electrode sites were simulated in each case and the duration of each recording was 5 minutes. One neuron was placed in the origin and approximately 600 noise neurons were placed at random positions, but at a minimum distance of 150μm from the target neuron. Each noise neuron was given a random mean firing rate between 1 and 50 spikes/second. A mean firing rate of 20 spikes/second was assigned to the target neuron. Spike times were generated by assuming gamma-distributed inter-spike intervals [13]. All spike times were stored at the time of simulation and used to extract spike waveforms.

### B. Feature-Space Representation of Spike Waveforms

The $P$-dimensional feature-space representation of sampled spike waveforms of length $N$ ($N$ = number of samples) was obtained by projecting the spike waveforms onto a set of $P$ ($P$ = number of feature space dimensions) $N$ sample long basis waveforms. To explore the effects of the selection of basis waveforms, we considered three sets of basis waveforms, where the $j$-th set of basis waveforms was contained in the columns of the $N \times P$ matrix $\boldsymbol{B}_j$. The columns of the matrix $\boldsymbol{B}_j$ were obtained as the first $P$ basis

waveforms from the principal component analysis of each of the following matrices:

1)  The matrix containing the mean spike waveforms in each electrode position in its columns (optimal basis).

2)  A matrix of the same size as that in 1), but whose elements were normally distributed random numbers (sub-optimal basis).

3)  The matrix containing the three very first waveforms in the first electrode position.

The $P \times M$ feature space representation $\boldsymbol{W}_j$ of the spike waveforms in the $N \times M$ matrix $\boldsymbol{S}$ in the space spanned by the basis waveforms in $\boldsymbol{B}_j$ was thus obtained through the projection and normalization

$$W_j = \frac{B_j^T S}{\left\| B_j^T S \right\|_2} \qquad (1)$$

where $\left\| . \right\|_2$ denotes the Euclidean norm.

### C. Comparison of Movement Paths between Spaces

To explore the similarity between electrode paths in the physical space and detected spikes in the feature space we defined the path measure $d$ that summarizes the path in a given $Q$-dimensional space ($Q > 1$) in a 1-dimensional sequence of normalized Euclidean distances of points along the path to the mean point of the path. For a path whose $i$-th coordinate in the original $Q$-dimensional space is given by $p_i$ and whose mean coordinate is given by $p_0$, the distance measure in the $i$-th point is given by

$$d_i = \left\| p_0 - p_i \right\|_2. \qquad (2)$$
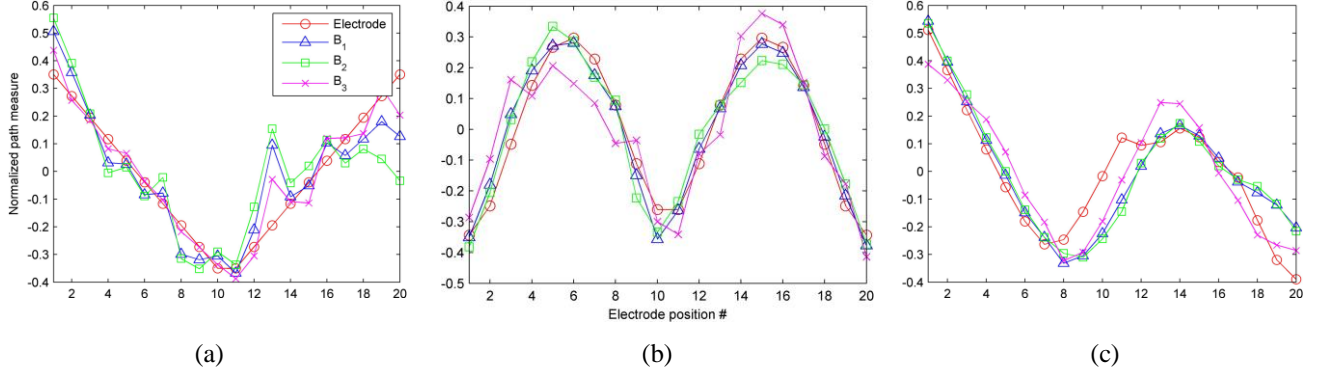
|  |  |  |
|---|---|---|
| (a) | (b) | (c) |

Fig. 2. The path measure $d$ for the electrode movements and corresponding movements of mean spike waveforms in the feature spaces spanned by three different sets of basis waveforms. (a) Linear path, (b) elliptical path, (c) P-shaped path. The path measures in the feature spaces were in all cases similar to those in the electrode movement space.

The $i$-th point corresponds to electrode site $i$ out of 20. For the feature spaces, we only considered the first three dimensions in this comparison. All distance measure sequences were normalized by first subtracting their respective mean values and then dividing by the Euclidean norm of the resulting sequence.

Although interpreting these one-dimensional path measures in terms of actual paths in a three-dimensional space is not straight forward, especially for more complex paths, they do provide a means for assessing the geometrical similarity between two paths in separate domains.

### D. Spike-Feature Based Estimation of Electrode Position

Based on the observation that electrode movements along a given path are translated to spike waveform movements along a similar path in the feature space, we assumed that there existed a $P \times 3$ matrix $A$ that transformed the 3-dimensional vector of Cartesian electrode coordinates to corresponding $P$-dimensional spike waveform coordinates in the feature space. This transformation is described by the linear model

$$B^T S = A X + \eta \qquad (3)$$

where $B$ and $S$ are the basis- and spike waveform matrices respectively, $X$ is the matrix containing the Cartesian coordinates of the electrode positions and $\eta$ is a matrix containing noise or variations not captured by the transformation matrix.

For a known matrix of Cartesian measurement point coordinates $X_0$, a corresponding matrix of measured mean spike waveforms $S_0$ and a set of basis waveforms $B$, an estimator for the transformation matrix is obtained by multiplying both sides of Eq. 3 by the Moore-Penrose psesudoinverse [14] of the Cartesian coordinate matrix, $X^+$, so that $X X^+ = I$, from the right, or

$$\widehat{A} = B^T S_0 X_0^+. \qquad (4)$$

Having obtained the estimate for the transformation matrix, it can now be used to estimate the electrode position for a given set of measured mean spike waveforms $S$ by multiplying Eq. 3 with the Moore-Penrose pseudoinverse of the estimated transformation matrix from the left, or
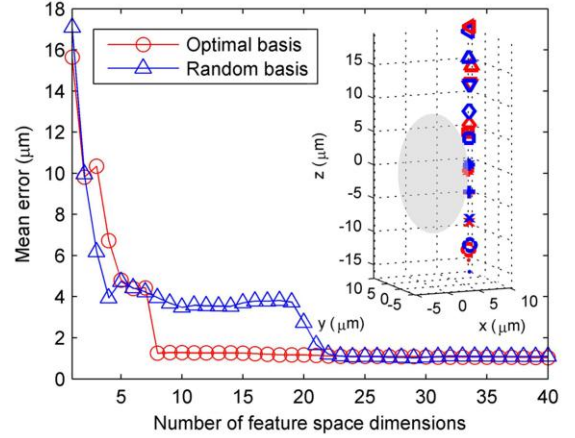


Fig. 3. Feature-space based estimation of electrode position during linear movement. The mean positioning error generally converged to a minimum value for both the optimal basis (obtained through PCA of the entire set of mean waveforms in training positions) and the random basis (obtained through PCA of a random matrix). However, the random basis generally converged at a higher number of dimesion. The inset shows the true (red) and estimated (blue) positions when using the 40-dimensional optimal basis. For the sake of clarity, the position of each channel is indicated by a specific symbol.

$$\widehat{X} = \widehat{A}^+ B^T S. \qquad (5)$$

To perform and evaluate feature space based electrode positioning, we divided the test data for the linear electrode movement (Sec. II-A) into two parts – odd-numbered channels (training data) and even-numbered channels (test data). The mean spike waveforms and Cartesian electrode coordinates of the odd-numbered channels, $S_0$ and $X_0$ respectively, were used for estimating the transformation matrix according to Eq. 4. This corresponds to a training period during which the position of the electrode is known. The resulting transformation matrix was then used to estimate the electrode positions of the even number channels $X$ by projecting the corresponding mean waveforms $S$ onto the basis that was used to estimate the transformation matrix according to Eq. 5.

To examine the sensitivity of positioning to the choice of basis waveforms and the number of basis waveforms

(number of feature space dimensions), we performed the above procedure using the optimal basis and the random basis (Sec. II-B) while successively increasing the number of dimensions and calculating the estimation error. The estimation error for each case was taken as the mean distance between true and estimated positions across all sites for that case.

## III. Results

### A. Comparison of Movement Paths

Fig. 2 shows the path measure $d$ that characterizes the electrode movements and the movements of the spike-features of mean waveforms in the feature spaces spanned by the three different bases described in Sec. II-B. In all feature spaces, the path measure was similar to that of the electrode path, indicating that electrode movements gave rise to similar spike movements in feature space. This was evident even for the random basis.

Increasing the length of the time spent in each position (T in Fig. 1 (d)), and thus increasing the number of spike waveforms used for forming the mean waveform in each position, increased the similarity between the path measures. As expected, the random basis required the largest number of waveforms to reach the high similarity shown in Fig. 2. The figure shows the case where the maximum amount of time is spent in each channel (T = 15 seconds).

### B. Spike-Feature Based Estimation of Electrode Position

Fig. 3 shows the mean estimation error (in μm) as a function of the number of feature space dimensions used in the electrode position estimation for the optimal basis and one realization of a random basis. The inset illustrates the true and estimated positions obtained using the 40-dimensional optimal basis.

The estimation error converged at approximately 8 dimensions when using the optimal basis. For the random basis, this limit was dependent on the realization, sometimes being lower than 8 and sometimes higher. In the case show in Fig. 3 the error converged at approximately 22 dimensions to approximately the same error as that obtained by using the optimal basis. For the case studied, the error converged onto a value of approximately 1μm.

## IV. Conclusion

In this paper we have presented preliminary findings regarding the relationship between physical movements of a recording electrode in extracellular neural recordings and the corresponding movement of spike-features in a feature space spanned by various basis waveforms. We have shown that there appears to be a characteristic relationship between the movements in these two domains and that this relationship can be interpreted as a linear transformation between two coordinate systems, not necessarily of equal dimensions. We have shown that, for linear electrode movements, this transformation can be acquired during a training period and then applied to estimate electrode position based on the feature space representation of spike waveforms. Due to the

introduction of a training procedure during electrode insertion, no prior information about the type of neuron is required. In our study, placing the electrode in the odd-numbered locations corresponds to the training period.

Future work involves verification of our findings by *in vivo* experiments, the full implementation of a practical framework for acquiring the coordinate transformation during electrode implantation and the utilization of the acquired transformation for post-implantation assessment of electrode movements. Future work also involves the utilization of this type of modeling for the purpose of tracking identified units between recording sessions.

Although the present study only addresses electrode positioning along a linear path, our results indicate that the estimation procedure is directly applicable during three-dimensional electrode movements. However, this has not been confirmed and thus requires further investigation.

## References

[1]    G. Buzsáki, "Large-scale recording of neuronal ensembles.," *Nature neuroscience*, vol. 7, no. 5, pp. 446-51, May 2004.

[2]    P. Mitra and H. Bokil, *Observed Brain Dynamics*. Oxford University Press, 2007, p. 408.

[3]    S. F. Lempka, M. D. Johnson, M. A. Moffitt, K. J. Otto, D. R. Kipke, and C. C. McIntyre, "Theoretical analysis of intracortical microelectrode recordings.," *Journal of neural engineering*, vol. 8, no. 4, p. 045006, Aug. 2011.

[4]    I. Obeid and P. D. Wolf, "Evaluation of spike-detection algorithms for a brain-machine interface application.," *IEEE transactions on bio-medical engineering*, vol. 51, no. 6, pp. 905-11, Jun. 2004.

[5]    M. S. Lewicki, "A review of methods for spike sorting: the detection and classification of neural action potentials.," *Network (Bristol, England)*, vol. 9, no. 4, pp. R53-78, Nov. 1998.

[6]    C. Gold, D. a Henze, and C. Koch, "Using extracellular action potential recordings to constrain compartmental models.," *Journal of computational neuroscience*, vol. 23, no. 1, pp. 39-58, Aug. 2007.

[7]    K. H. Pettersen and G. T. Einevoll, "Amplitude variability and extracellular low-pass filtering of neuronal spikes.," *Biophysical journal*, vol. 94, no. 3, pp. 784-802, Feb. 2008.

[8]    A. Bar-Hillel, A. Spiro, and E. Stark, "Spike sorting: Bayesian clustering of non-stationary data.," *Journal of neuroscience methods*, vol. 157, no. 2, pp. 303-16, Oct. 2006.

[9]    F. Franke, M. Natora, C. Boucsein, M. H. J. Munk, and K. Obermayer, "An online spike detection and spike classification algorithm capable of instantaneous resolution of overlapping spikes.," *Journal of computational neuroscience*, vol. 29, no. 1-2, pp. 127-48, Aug. 2010.

[10]   P. T. Thorbergsson, M. Garwicz, J. Schouenborg, and A. J. Johansson, "Computationally efficient simulation of extracellular recordings with multielectrode arrays (submitted manuscript)," 2012.

[11]   M. L. Hines and N. T. Carnevale, "The NEURON Simulation Environment," *Neural Computation*, vol. 9, no. 6, pp. 1179-1209, Aug. 1997.

[12]   C. Gold, D. a Henze, C. Koch, and G. Buzsáki, "On the origin of the extracellular action potential waveform: A modeling study.," *Journal of neurophysiology*, vol. 95, no. 5, pp. 3113-28, May 2006.

[13]   D. Heeger, "Poisson model of spike generation," *Handout, University of Standford*, pp. 1-13, 2000.

[14]   C. Meyer, "Matrix Analysis and Applied Linear Algebra. 2000," *SIAM, Philadelphia*, vol. 1, no. 11, pp. 1829–1841, 2004.